RESEARCH ARTICLE | JUNE 02 2025

Additive strategy for nucleation pathway control based on the understanding of molecular size effect on crystallization

Yuya Iida ; Shotaro Hiraide ; Satoshi Watanabe

J. Chem. Phys. 162, 214503 (2025)
https://doi.org/10.1063/5.0266286

The Journal of Chemical Physics ARTICLE pubs.aip.org/aip/jcp

Additive strategy for nucleation pathway control based on the understanding of molecular size effect on crystallization

Cite as: J. Chem. Phys. 162, 214503 (2025); doi: 10.1063/5.0266286
Submitted: 18 February 2025 • Accepted: 9 May 2025 •
Published Online: 2 June 2025

Yuya Iida,[1] Shotaro Hiraide,[1,2] and Satoshi Watanabe[1,a)]

AFFILIATIONS

[1] Department of Chemical Engineering, Kyoto University, Katsura, Nishikyo, Kyoto 615-8510, Japan
[2] Institute for Aqua Regeneration, Shinshu University, 4-17-1 Wakasato, Nagano 380-8553, Japan

[a)] Author to whom correspondence should be addressed: nabe@cheme.kyoto-u.ac.jp

ABSTRACT

Understanding mechanisms involved in particle formation processes is crucial to effectively control crystalline particle characteristics. This study highlights the significan effect of slight changes in molecular size on the crystallization pathway. Molecular dynamics simulations are performed in a binary Lennard-Jones system as a model for systems that undergo two-step nucleation via an intermediate droplet structure. This study analyzed two cases with different solute–solute interaction strengths and found that a larger solute-to-solvent size ratio delayed droplet crystallization in both cases. In systems with strong solute–solute interactions, this delay shifted the pathway from one-step-like to two-step-like nucleation, as droplets with larger solute molecules incorporated more solvent, thereby hindering crystallization. We explained this change in droplet composition by considering the mixing free energy between the solute and solvent. Larger solute molecules form entropically and enthalpically favorable structures by accommodating solvent molecules, which increase the solvent fraction of the droplet. We used a thermodynamic model based on the classical nucleation theory with a core–shell nucleus and revealed that this increased solvent fraction in the droplet lowered the freezing point of the droplet and raised the solid–liquid interfacial tension, ultimately delaying and suppressing crystallization. Based on these findings we proposed a strategy to control the nucleation pathway using additives. Introducing appropriate additives to modify the stability of intermediates is a promising strategy to control nucleation pathways in various systems.

I. INTRODUCTION

Particles are fundamental materials in numerous industries, and precise control over their properties is critical across diverse fields including chemistry,[1,2] pharmaceuticals,[3,4] and electronics.[5,6] However, the limited understanding of the initial nucleation process in particle formation results in the synthesis process heavily relying on trial-and-error approaches, making the development of universal and versatile methods for particle synthesis an ongoing challenge.

The limited progress in understanding nucleation can be attributed to challenges associated with nucleation proceeding via various pathways. Traditionally, it has been assumed that nucleation follows a one-step pathway, as described by the classical nucleation theory (CNT).[7] In this pathway, monomers form nuclei that possess identical structures as fina particles, which then grow through the addition of individual monomer units. In contrast, many systems pass through intermediate states with structures distinct from the fina particle. Representative examples include the two-step nucleation pathway,[8–12] where crystallization occurs from droplets formed via liquid–liquid phase separation (LLPS) or other mechanisms, and the pre-nucleation cluster (PNC) pathway,[13–18] where monomer molecules or ions in the solution form PNCs made of highly dynamic polymer-like chains, as observed in biomineralization. Furthermore, in some cases, the growth units exceed the size of individual monomers,[19–22] with oligomers or primary particles aggregating to play a central role in particle formation. This diversity of pathways complicates the efforts toward the systematic understanding and theoretical description of nucleation processes.

Although diversity of particle formation pathways poses challenges for understanding particle formation mechanisms, it simultaneously offers opportunities for the tailored design of particles. For instance, the two-step nucleation pathway via LLPS enables the production of unique shapes, sizes, and surface morphologies[23–26] unattainable through the conventional one-step pathway. Furthermore, this pathway has been utilized for the one-pot synthesis of spherical particle aggregates by leveraging the strong aggregation tendency of particles within droplets.[27,28] Similarly, multiple studies have suggested that the structure of the initially formed PNCs in the PNC pathway dictates the fina polymorphism of the particles.[13,29,30] Mastering control over these pathways can provide a powerful tool for tailoring particle size, shape, and polymorphism and achieving precise particle design.

Thus far, several studies have demonstrated that the nucleation pathway can change depending on the synthesis conditions, thereby providing potential strategies for pathway control. Temperature is a well-studied parameter,[31–36] with several reports on systems exhibiting a one-step pathway at low temperatures and a two-step pathway at high temperatures,[31,34] and vice versa.[33,36] Salvalaglio *et al.* performed molecular dynamics (MD) simulations, which revealed that urea nucleates through a one-step pathway in water and acetonitrile, whereas a two-step pathway occurs in ethanol and methanol, thereby highlighting the significanc of solvent effects.[37,38] Similarly, in biomineral systems displaying the PNC pathway, conventional one-step nucleation can emerge under specifi concentration conditions or in the presence of substrates that promote heterogeneous nucleation.[39,40] In addition, in cobalt and PbS nanoparticle systems, the pathway involving intermediate structures transitions to a one-step pathway when certain additives are introduced.[41,42]

The pathway change depending on synthesis conditions can be attributed to the alteration of the thermodynamic or kinetic state of the intermediate structure. Deepening the understanding of the relationship between the characteristics of relevant molecules and environmental conditions, state of the intermediate structure and its crystallization behavior is essential for effectively controlling the pathway. To this end, we have simulated the nucleation process in a binary Lennard-Jones (LJ) system,[43,44] which serves as a model for systems that undergo crystallization via an intermediate structure. The LJ systems can be considered a simple model where the solute and solvent are represented as coarse-grained molecules. Researchers widely used this system to derive universal insights related to solvation,[45] secondary nucleation,[46] effects of additives,[47] and antisolvent crystallization.[48] In our previous work, a two-step nucleation pathway associated with droplet formation via LLPS was observed.[43] When the solute and solvent are of equal size, the system tends toward a one-step pathway with immediate crystallization following droplet formation under conditions of strong supercooling (either low temperature or high solute–solute interaction). Furthermore, we discovered that even a slight difference in molecular size can cause the droplet formation rate to vary by several orders of magnitude.[44] Similar to its effect on the droplet formation, the firs stage of the two-step nucleation, changes in molecular size significantly affect both droplet structure and crystallization behavior. However, systematic investigations into the effect of molecular size on droplet crystallization remain largely unexplored. In this study, we systematically evaluate the effect of molecular size on the crystallization of droplets formed from a supersaturated solution in the binary LJ system. The simulation results indicate that molecular size variations alter the composition of the droplets, which affects their propensity for crystallization. These changes in droplet composition and crystallization barriers are rationally explained by theoretical consideration based on mixing free energy change and the thermodynamic model introduced in our previous study. We provide a microscopic picture of mechanisms behind droplet composition variation and offer thermodynamic explanations for changes in crystallization barriers. In addition, we discuss strategies to control the nucleation pathway using additives based on the finding presented in this study. Our results confir that changing the stability of the intermediate structure using additives is an effective and universal strategy for pathway control.

II. METHODS

A. Molecular dynamics simulation

We conducted MD simulations in the same binary LJ systems composed of 1500 solute molecules A and 24 000 solvent molecules B, as those reported in our previous studies.[43,44] The two-body interaction, ϕ_{ij}, of LJ molecule is given by

$$\phi_{ij} = 4\varepsilon\left[\left(\frac{\sigma}{r_{ij}}\right)^{12} - \left(\frac{\sigma}{r_{ij}}\right)^{6}\right], \tag{1}$$

where r_{ij} represents the distance between molecules i and j, and σ and ε are LJ parameters representing the effective molecular size and strength of the interaction, respectively. The LJ parameters of the solutes and solvents used in this study are summarized in Table I. We varied the size ratio of the solute to the solvent, σ_{AA}/σ_{BB}, by varying the solvent size under two parameter sets with different values of solute–solute interaction strength $\varepsilon^*_{AA} = \varepsilon_{AA}/k_BT$ (Table I parameter sets 1 and 2) to systematically investigate the effects of interaction parameters on the crystallization step of the two-step nucleation. The strengths of solvent–solvent interaction ε^*_{BB} and solute–solvent ε^*_{AB} were selected so that the values of $\Delta\varepsilon^* = \varepsilon^*_{AA} + \varepsilon^*_{BB} - 2\varepsilon^*_{AB}$ for the two parameter sets were the same because our previous study demonstrated that $\Delta\varepsilon^*$ governs the droplet formation process for a system with an identical molecular size ($\sigma_{AA} = \sigma_{BB} = \sigma_{AB}$).[43] We performed at least 20 simulation runs up to 500 ns with different initial solution configuration for a single condition to cope with the stochastic nature of nucleation. We calculated and traced the number of solute molecules in the largest assembled structure n_L and that in the largest crystal n_C based on the procedure proposed by Tribello *et al.*[49] to detect the droplet formation and its crystallization. Droplet formation and crystallization were define as the point at which n_L

TABLE I. LJ parameters of the solutes and solvents.

	$\varepsilon^* = \varepsilon/k_BT$ [−]				σ[Å]		
	ε^*_{AA}	ε^*_{BB}	$\Delta\varepsilon^*$	(ε^*_{AB})	σ_{AA}	σ_{AA}/σ_{BB} [−]	σ_{AB}
Set 1	2.0	1.34	0.67	(1.34)	3.0	0.85–1.15	$\frac{\sigma_{AA}+\sigma_{BB}}{2}$
Set 2	2.67			(1.67)			

and n_C satisfie a specifi condition (detailed definition are provided in the Appendix), thereby ensuring that the droplet and the crystal reached a certain size and did not redissolve. The induction time for crystallization t_C was then calculated as the time elapsed from droplet formation to crystallization for each simulation run. The average induction time τ_C was estimated from 20 or more simulation runs assuming a Poisson process to deal with the stochasticity of nucleation (detailed calculation procedures of the induction time and its average are provided in the Appendix). All simulation runs were performed in the NpT ensemble at 180 K and 0.77 kbar using the velocity rescaling thermostat[50] and Parrinello–Rahman barostat[51] of the open-source simulator GROMACS (version 2019.4).[52] Periodic boundary conditions were applied in all three directions of a cubic cell with dimensions of ~$9 \times 9 \times 9$ nm^3, and the time step was set to 2 fs. The LJ-potential was cut and shifted at $4\sigma_{max}$ [$\sigma_{max} = \max(\sigma_{AA}, \sigma_{BB})$]. The calculation of n_L and n_C was performed using the PLUMED software package (version 2.5.4).[53]

1. Calculation of the solvent fraction in the liquid droplet

The solvent fraction in a liquid droplet was calculated from the simulation results using two distinct procedures depending on droplet size and its stability. For parameter set 1, where the droplet size was almost constant over a certain period of the simulation, we computed radial profile of local solvent fraction by counting the number of solute and solvent molecules within each spherical shell at a certain distance from the center of mass of the droplet. Then, the resulting radial profil was fitte to a hyperbolic tangent function with an offset. The solvent fraction in the droplet x_{Bs} was determined as the value of the fittin curve at the center [See Fig. 5(c)].

For parameter set 2, where obtaining reliable statistics for the radial profil of the local solvent fraction was difficul due to droplet instability, we estimated x_{Bs} by directly counting the number of solvent molecules n_B within the droplet. A solvent molecule within the droplet was define as the molecule coordinated by more than m solute molecules comprising the droplet. The solvent fraction in the droplet x_{Bs} was computed as the ensemble average of $n_B/(n_L + n_B)$ for states where $n_L \geq 100$ prior to crystallization. The appropriate value of m varied with the solute-to-solvent size ratio, and we determined the optimal m value by comparing the x_{Bs} results obtained from this direct counting method with those from the fitting-base method for parameter set 1. m values that yielded the closest x_{Bs} values between the two procedures for parameter set 1 were selected for each solute-to-solvent size ratio. The cutoff distance for coordination was set at $1.3\sigma_{ij}$. The analyses explained here were performed using the visualization and analysis software OVITO.[54]

B. Thermodynamic model

1. Solvent fraction within the liquid droplet

We theoretically predicted x_{Bs} by calculating the mixing free energy change of solute and solvent molecules. Under the constant N, p, and T conditions, ΔG_{mix} is expressed as

$$\Delta G_{mix} = \Delta H_{mix} - T\Delta S_{mix}, \tag{2}$$

where ΔH_{mix} and ΔS_{mix} represent enthalpy change and entropy change by mixing, respectively. By approximating the LJ binary solution as a regular solution, in which only dispersion forces act as attractive forces, ΔH_{mix} and ΔS_{mix} are given by[55]

$$\Delta H_{mix} = (N_A + N_B)\frac{x_A V_A x_B V_B}{x_A V_A + x_B V_B} \times \left\{\frac{\Delta H_A - k_B T}{V_A} + \frac{\Delta H_B - k_B T}{V_B} - \frac{2(\Delta H_{AB} - k_B T)}{V_{AB}}\right\}, \tag{3}$$

$$\Delta S_{mix} = -(N_A + N_B)k_B(x_A \ln x_A + x_B \ln x_B), \tag{4}$$

where V_i (i = A, B, AB) represents the volume per molecule, ΔH_i represents evaporation enthalpy per molecule, k_B represents the Boltzmann constant, and i = AB represents the average properties as a mixture. By expressing the ratio of each V_i and ΔH_i using molecular size σ and interaction strength ε as $V_B/V_A = (\sigma_{BB}/\sigma_{AA})^3$, $V_{AB}/V_A = (\sigma_{AB}/\sigma_{AA})^3$, and $\Delta H_i/k_B T = Z_v \varepsilon_i^*$, ΔH_{mix} is rewritten as

$$\Delta H_{mix} = (N_A + N_B)k_B T\beta\left[\frac{x_A r x_B}{x_A + r x_B}\right], \tag{5}$$

where

$$\beta = Z_v\left\{\varepsilon_{AA}^* + \left(\frac{\sigma_{AA}}{\sigma_{BB}}\right)^3\varepsilon_{BB}^* - 2\left(\frac{\sigma_{AA}}{\sigma_{AB}}\right)^3\varepsilon_{AB}^*\right\} - \left\{1 + \left(\frac{\sigma_{AA}}{\sigma_{BB}}\right)^3 - 2\left(\frac{\sigma_{AA}}{\sigma_{AB}}\right)^3\right\}, r = \left(\frac{\sigma_{BB}}{\sigma_{AA}}\right)^3.$$

When a homogeneous solution is unstable, the solute and solvent spontaneously separate into two phases, whose solute fractions are x_{A1} and x_{A2} ($x_{A2} > x_{A1}$). The two separated phases have identical chemical potential that minimizes the free energy of the whole system, and therefore, x_{A1} and x_{A2} have to satisfy

$$\begin{cases} \left.\frac{\partial \Delta G_{mix}}{\partial x_A}\right|_{x_{A1}} = \left.\frac{\partial \Delta G_{mix}}{\partial x_A}\right|_{x_{A2}}, \\ \left.\frac{\partial \Delta G_{mix}}{\partial x_A}\right|_{x_{A1}} = \frac{\Delta G_{mix}(x_{A2}) - \Delta G_{mix}(x_{A1})}{x_{A2} - x_{A1}}. \end{cases} \tag{6}$$

We calculated $x_{Bs} = 1 - x_{A2}$ by solving Eq. (6).

2. Free energy barrier for droplet crystallization

We calculated the free energy barrier for crystallization from n_L-sized droplets to theoretically examine the induction time of crystallization. As shown in Fig. 1, the formation of a crystal nucleus with a number of molecules n_C inside a droplet containing n_L monomer molecules is represented by the difference between two processes: (1) the formation of a droplet nucleus from a homogeneous solution and (2) the formation of a core–shell nucleus, which includes a crystal core and a solute-rich phase shell, from a homogeneous solution. Therefore, the free energy change caused by the formation of the crystal nucleus within a n_L-sized droplet ΔG_C can be calculated by

$$\Delta G_C(n_L, n_C) = \Delta G(n_L, n_C) - \Delta G(n_L, 0), \tag{7}$$

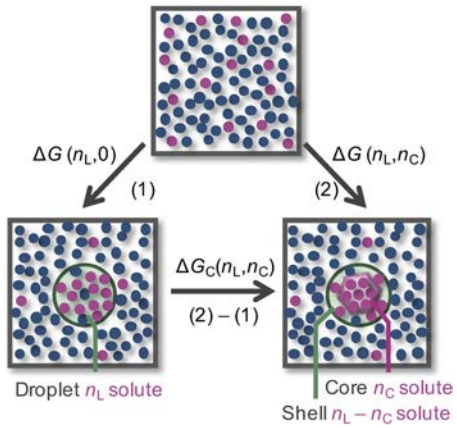

FIG. 1. Schematic of the free energy change for the formation of a crystal nucleus within a droplet.

where $\Delta G(n_L, n_C)$ is the free energy change due to formation of a core–shell nucleus with a n_C-sized core and a $(n_L - n_C)$-sized shell from the initial solution phase. We can calculate $\Delta G(n_L, n_C)$ through a model that we developed in our previous study,[43] which provides $\Delta G(n_L, n_C)$ as a function of interaction parameters ε^* and σ [detailed expression of $\Delta G(n_L, n_C)$ is provided in the Appendix]. The free energy barrier for droplet crystallization ΔG_C^{max} was calculated as the maximum of $\Delta G_C(n_L, n_C)$ at a constant n_L. The values obtained from the MD simulations were used for the x_{Bs} values required for the $\Delta G(n_L, n_C)$ calculation.

III. RESULTS AND DISCUSSION

A. Simulation results

Figure 2 shows typical time courses of n_L and n_C of the simulations for parameter sets 1 and 2 with σ_{AA}/σ_{BB} = 0.90, 1.0, and 1.10 (A: solute, B: solvent). In parameter set 1, where the solute–solute interaction is weak, we observed typical two-step nucleation behaviors for all σ_{AA}/σ_{BB} values. A solute-rich liquid droplet formed from the initial solution state ($n_L \simeq 0$, $n_C \simeq 0$), which was detected by the rapid increase in n_L. The droplet size remains unchanged for a certain induction time t_C, and then, it crystallized with a steep increase in n_C. t_C significantl increased for σ_{AA}/σ_{BB} = 1.10 compared to σ_{AA}/σ_{BB} = 0.90 and 1.0. In parameter set 2, where the solute–solute interaction is strong, we observed one-step-like nucleation characterized by the instantaneous crystallization of the liquid droplet. The liquid droplet did not reach a plateau size because it crystallized at a considerably earlier stage of droplet growth than that for parameter set 1. The driving force of LLPS became larger for a strong solute–solute interaction with a small σ_{AA}/σ_{BB}, as demonstrated in our previous study.[44] The results of a smaller σ_{AA}/σ_{BB} showed a stair-like increase in n_L and n_C because of the formation of multiple particles and their subsequent coalescence. Furthermore, crystallization occurred at a slightly larger size of the liquid droplet with an increase in σ_{AA}/σ_{BB}, as indicated by the black circles in Fig. 2(b). These results suggest that the larger solute size compared to the solvent molecules delays the crystallization of the droplet.

This tendency was confirme by calculating the average induction time for crystallization τ_C and the mean droplet size at initial crystallization n_L^{cryst} for each σ_{AA}/σ_{BB} value, which are shown in Fig. 3. τ_C was almost constant for all size ratios when $\sigma_{AA}/\sigma_{BB} \leq 1$, whereas it increased by several orders of magnitude as

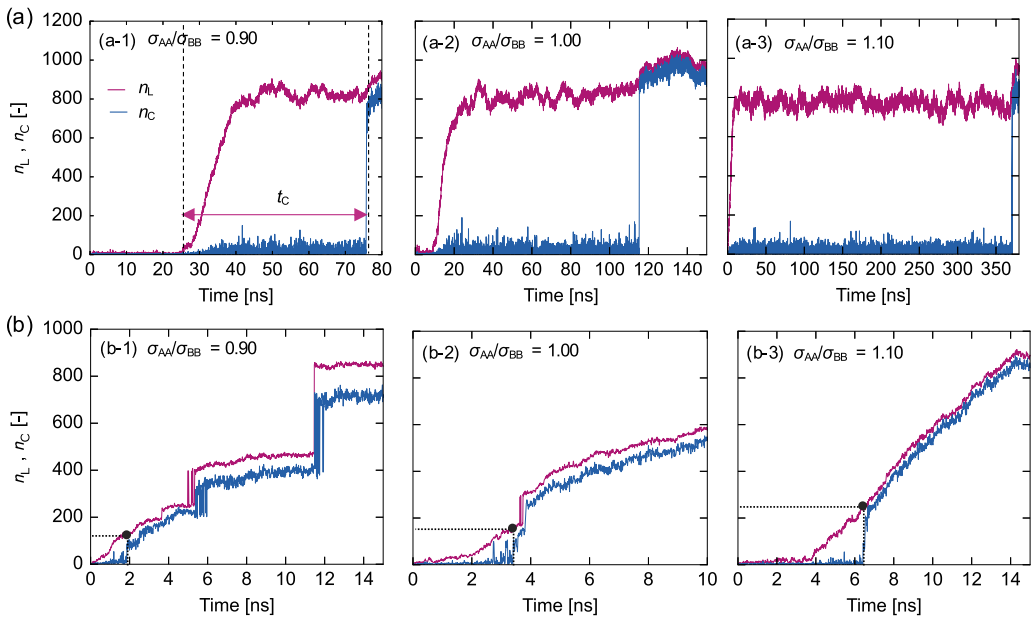

FIG. 2. Typical time courses of n_L and n_C for (a) parameter set 1: ε^*_{AA} = 2.0, with σ_{AA}/σ_{BB} = 0.90, 1.0, and 1.10 and (b) parameter set 2: ε^*_{AA} = 2.67, with σ_{AA}/σ_{BB} = 0.90, 1.0, and 1.10. The black circles in panel (b) indicate n_L at the initial crystallization.

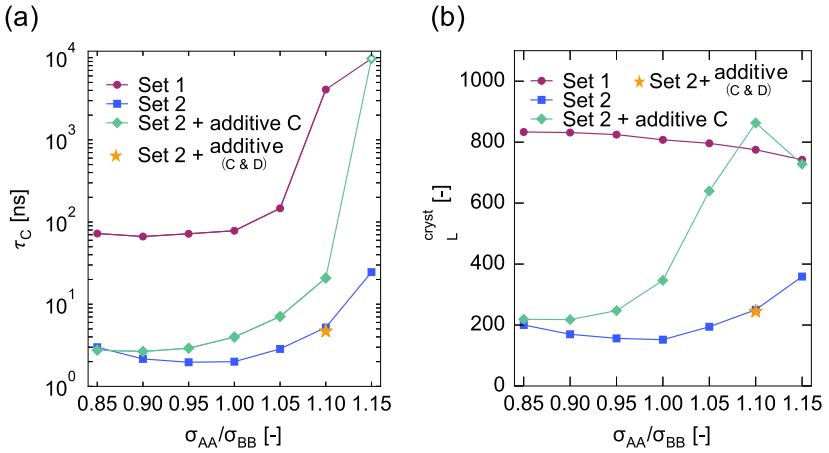

FIG. 3. (a) Average induction time for crystallization τ_C and (b) mean droplet size at the initial crystallization n_L^{cryst} for each σ_{AA}/σ_{BB} value in parameter sets 1 and 2, and under conditions where additives were added to the parameter set 2 system. Crystallization was not observed within a 500 ns simulation time in any 20 runs for $\sigma_{AA}/\sigma_{BB} = 1.15$ of parameter set 1 and the additive system, and therefore, the corresponding data points are a lower limit of τ_C estimated by using the method described in the Appendix (indicated by open plots).

σ_{AA}/σ_{BB} increased when $\sigma_{AA}/\sigma_{BB} \geq 1$ for both parameter sets. For $\sigma_{AA}/\sigma_{BB} = 1.15$ of parameter set 1, we could not observe crystallization within the 500 ns simulation time in any 20 runs, although the control study that started from a crystal showed that the crystal state is most stable. The mean droplet size n_L^{cryst} for parameter set 2 followed a similar trend to that of τ_C. n_L^{cryst} increased with an increase in σ_{AA}/σ_{BB} in the range of $\sigma_{AA}/\sigma_{BB} \geq 1$. The slight increase in n_L^{cryst} in smaller σ_{AA}/σ_{BB} can be attributed to the coalescence of multiple droplets inducing a temporary formation of a large droplet and its immediate crystallization. For parameter set 1, n_L^{cryst} was ~800 for all σ_{AA}/σ_{BB} because the droplet size reached the stable size determined by the finit system size.

We investigated the structure of the droplet to clarify the mechanism of the crystallization suppression observed for $\sigma_{AA}/\sigma_{BB} \geq 1$. Figure 4(a) shows the pair distribution function of the solute molecule when the droplet remains in the plateau size in parameter set 1. The height of each peak decreased with an increase in σ_{AA}/σ_{BB}, indicating that the solute molecules become less likely to form the local positional order. This decreasing rate was larger in the range of $\sigma_{AA}/\sigma_{BB} \geq 1$, as depicted in Fig. 4(b). This implies the existence of something that disturbs the development of the local order in the droplet of larger solute molecules, potentially explaining the observed trends in τ_C and n_L^{cryst}.

Figures 5(a) and 5(b) show the snapshots of the droplet for $\sigma_{AA}/\sigma_{BB} = 0.85$ and 1.15 in parameter set 1. As clearly indicated by the snapshots, the droplet of larger solute molecules [Fig. 5(b), $\sigma_{AA}/\sigma_{BB} > 1$] contains a significan amount of solvent molecules, whereas that of smaller solute molecules [Fig. 5(a), $\sigma_{AA}/\sigma_{BB} < 1$] is an almost pure solute droplet. We quantitatively confirme it by calculating the solvent fraction in the droplet x_{Bs}. Radial profile of the solvent fraction are plotted in Fig. 5(c). The solvent fraction smoothly decreases from the solution bulk to the droplet surface and becomes a plateau at the center of the droplet. Each profil was well fitte to a hyperbolic tangent function with an offset. Figure 5(d) shows x_{Bs} values obtained from this fitting-base method for parameter set 1 and those from the direct counting method for parameter set 2. A larger value of σ_{AA}/σ_{BB} results in a larger x_{Bs} value, which implies that solvent molecules enclosed in the droplet disturb the development of the local order and suppress the crystallization. Solvent molecules incorporated into the droplet tended to be expelled during crystal nucleation within the droplet. However, some remained trapped within the crystal lattice, particularly under larger σ_{AA}/σ_{BB} conditions. In parameter set 2, where both solute–solute (ε^*_{AA}) and solute–solvent (ε^*_{AB}) interactions are strong, once solvent molecules were incorporated into the crystal surface, they were less likely to escape. Consequently, even if solvent molecules were not captured during nucleation within the droplet, they were often incorporated into the crystal structure during subsequent growth.

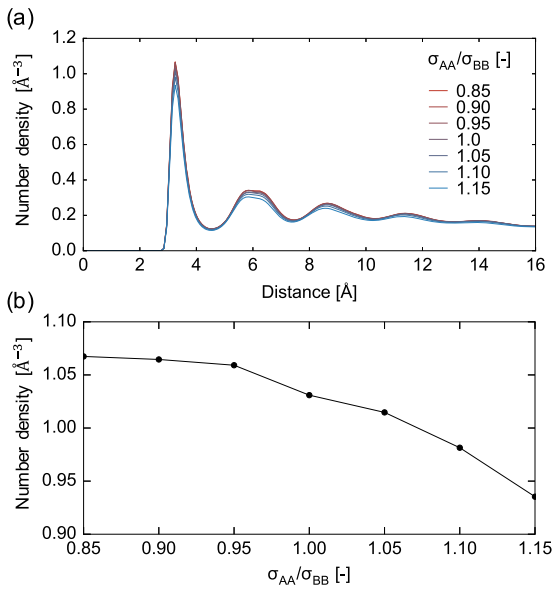

FIG. 4. (a) Pair distribution function of solute molecule when the droplet maintains a stable size in parameter set 1. (b) Height of the firs peak of the pair distribution function as a function of σ_{AA}/σ_{BB}.

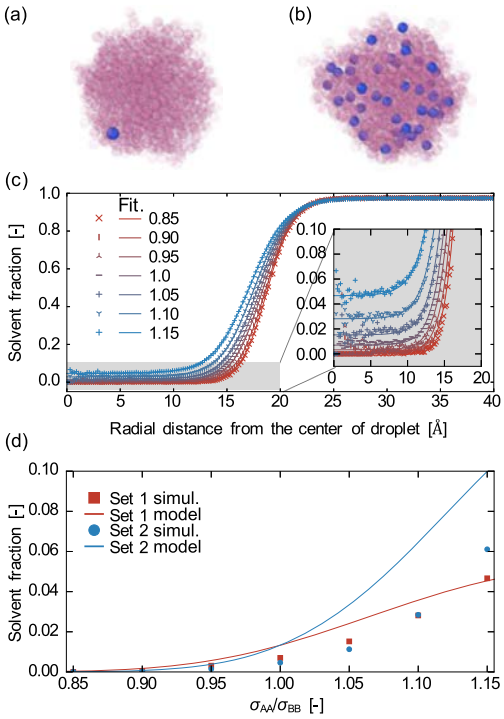

FIG. 5. (a) Snapshots of the droplet for σ_{AA}/σ_{BB} = 0.85 and (b) 1.15 in parameter set 1 (solute: transparent pink, solvent: blue). (c) Radial profile of solvent fraction in the droplet in parameter set 1 and (d) solvent fraction in the droplet x_{Bs} for parameter set 1 and 2 obtained from the MD simulation and mixing free energy, respectively. The values of m were 12, 12, 10, 10, 9, 8, and 7 for σ_{AA}/σ_{BB} = 0.85, 0.90, 0.95, 1.0, 1.05, 1.10, and 1.15, respectively.

B. Microscopic mechanism of solvent fraction variation

We calculated x_{Bs} theoretically to understand the mechanism of the solvent fraction variation. Figures 6(a)–6(c) shows ΔG_{mix}, ΔH_{mix}, and ΔS_{mix} as a function of solute fraction x_A for σ_{AA}/σ_{BB} = 0.85, 1.0, and 1.15 in parameter set 1. A supersaturated system separates into two phases that satisfy Eq. (6), indicating that the two tangent points of the co-tangent line of the ΔG_{mix} vs x_A profile correspond to the stable compositions of the two phases. Compared to the ΔG_{mix} profil of σ_{AA}/σ_{BB} = 1, which is symmetric, that of σ_{AA}/σ_{BB} = 0.85 is shifted to the right and that of σ_{AA}/σ_{BB} = 1.15 to the left. Consequently, the right-hand tangent point corresponding to the solute fraction $x_{As}(= 1 - x_{Bs})$ of the droplet becomes smaller for a larger σ_{AA}/σ_{BB}. The solid lines in Fig. 5(d) represent the predicted x_{Bs} based on ΔG_{mix} for parameter sets 1 and 2. The predicted values successfully capture the trend of x_{Bs} increasing with an increase in σ_{AA}/σ_{BB}. The slight overestimation of x_{Bs} can be attributed to the inherent limitation of the regular-solution-based model, which accounts for interactions between the nearest neighboring molecules. As interactions beyond this range are neglected, deviations between the model and simulation results become more significan when the contributions of interactions with the non-nearest neighboring solutes increase. This aligns with the relatively larger discrepancy observed in set 2, where the solute–solute interaction strength is higher, thereby leading to a greater influ ence of non-nearest neighboring solute interactions than that of set 1.

The shifted ΔG_{mix} profile in $\sigma_{AA} \neq \sigma_{BB}$ solutions emerge because of the shift of ΔH_{mix} profiles Consequently, the difference in enthalpy (energy) gain or loss caused by mixing solute and solvent molecules is the origin of the differences in x_{Bs} by σ_{AA}/σ_{BB}, which can be explained by the following microscopic

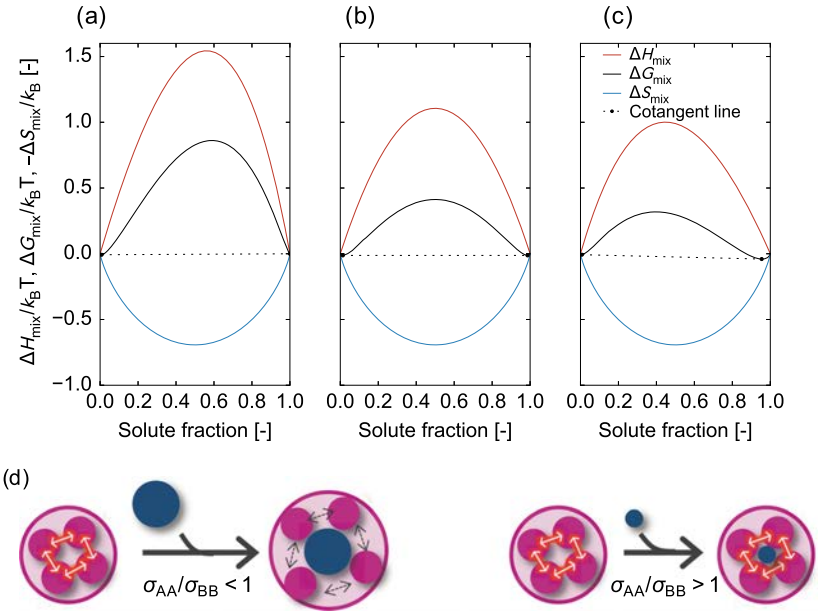

FIG. 6. Mixing free energy change ΔG_{mix}, enthalpy change ΔH_{mix}, and entropy change ΔS_{mix} as a function of solute fraction x_A for σ_{AA}/σ_{BB} = (a) 0.85, (b) 1.0, and (c) 1.15 in parameter set 1. (d) Schematic of microscopic changes that occur when a small amount of solvent is mixed with a pure solute domain.

changes that occur when solvents mix with pure solutes, as shown in Fig. 6(d): when a small amount of solvent is mixed with a pure solute domain, the system gains an entropic advantage because of an increased disorder. However, the solvent interrupts interactions between solute molecules, thereby leading to an enthalpic disadvantage. If the solvent molecules are large ($\sigma_{AA}/\sigma_{BB} < 1$), they disrupt the solute–solute interactions more effectively, thereby resulting in a greater enthalpic loss. This effect is reflecte in the steep slope of the ΔH_{mix} profil near $x_A = 1$ shown in Fig. 6(a). Conversely, when the solvent molecules are small, they can slip into the gaps between the larger solute molecules without fully severing their interactions, thereby enabling the system to gain the entropic benefi of mixing with minimal enthalpic cost. The gradual slope of the ΔH_{mix} profil near $x_A = 1$ shown in Fig. 6(c) demonstrates the lower enthalpic cost. Thus, the size ratio of the solute to the solvent molecules define the relative magnitude of enthalpic loss to entropic gain by mixing, which determines the solvent fraction in the droplet.

C. Free energy barrier for droplet crystallization

The suppression of crystallization caused by variations in solvent fraction is confirme by calculating the free energy barrier for droplet crystallization ΔG_C^{max}. Figure 7 shows ΔG_C^{max} as a function of n_L for each σ_{AA}/σ_{BB} in parameter sets 1 (solid line) and 2 (dashed line). The star markers indicate the ΔG_C^{max} values at n_L^{cryst} observed in the MD simulation. The freezing point depression caused by the Gibbs–Thomson effect, which hinders crystal nucleus formation, is more pronounced in smaller droplets,[56] and therefore, the crystallization barrier decreases with an increase in the droplet size. Regardless of σ_{AA}/σ_{BB}, the nucleation barrier is higher in parameter set 1, where solute–solute interactions are weaker, compared to those in parameter set 2, which exhibits stronger solute–solute interactions. This trend aligns with the simulation results: in set 1, droplets grow to a plateau size of ~800 molecules before crystallization, while in set 2, crystallization occurs at a much smaller droplet size. As reflecte in the simulation results for τ_C and n_L^{cryst}, ΔG_C^{max} increases as σ_{AA}/σ_{BB} increases in both parameter sets. The resulting crystallization barrier is approximately the same ($\approx 10 k_B T$) for each

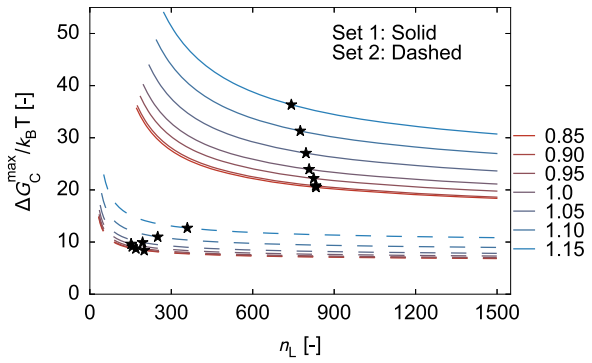

FIG. 7. Free energy barrier for droplet crystallization, ΔG_C^{max}, as a function of droplet size, n_L, for each σ_{AA}/σ_{BB} in parameter sets 1 and 2. The star markers indicate the ΔG_C^{max} values at n_L^{cryst} observed in the MD simulation.

σ_{AA}/σ_{BB} in parameter set 2, whereas in parameter set 1, the barrier at n_L^{cryst} is higher for conditions with a larger σ_{AA}/σ_{BB}. This reflect the difference in the stochastic nature of crystallization under the two parameter sets. The fluctuation in crystallization (temporary formation of crystalline domains within the droplet) increase as the droplet grows. For parameter set 2, the crystallization barrier of $\sim 10 k_B T$ is sufficientl low to be overcome by minor fluctuation in the growing droplet. Therefore, in parameter set 2, crystallization occurs almost deterministically when the droplet reaches a size where the fluctu ations are $\sim 10 k_B T$. In other words, in parameter set 2, the growth rate of the droplet is the rate-limiting factor for crystallization. In contrast, for parameter set 1, a higher crystallization barrier cannot be surmounted by the fluctuation of the growing droplet. Instead, crystallization occurs only after the droplet size reaches a plateau. In this case, the rate-limiting step is the formation of the critical crystal nucleus in the droplet rather than droplet growth, thereby making the stochastic nature of the process more prominent.

We discuss the relationship between the solvent fraction in the droplet and the crystallization barrier by rewriting Eq. (7) in a simplifie form for a sufficientl solute-rich droplet ($x_{Bs} < 0.1$). By neglecting the change in the concentration of the solution phase and the droplet diameter due to the formation of a crystal nucleus inside the droplet, we obtain the following simplifie expression for ΔG_C from Eqs. (7), (A4), (A5), and (A7):

$$\Delta G_C \simeq n_C k_B T \times \left[-Z_m \varepsilon_{AA}^* \left(1 - \frac{T}{T_m(n_L)} \right) - \ln(1 - x_{Bs}) - \beta \phi_{Bs}^2 \right] + \gamma_C(x_{Bs}) a_C^{2/3} n_C^{2/3}, \quad (8)$$

where $T_m(n_L)$ represents the freezing point of an n_L-sized droplet, as given by Eq. (A6), which incorporates the Gibbs–Thomson effect; Z_m represents the fusion enthalpy of the LJ molecules scaled by ε; ϕ_{Bs} represents the volume fraction of solvent in the droplet; $a_C = 6\sqrt{\pi} v_C$; v_C represents occupied volume per solute molecule in a crystal; and γ_C represents the crystal–droplet (shell) interfacial tension. The firs term is stabilization by crystal phase formation, and the second term is energy penalty attributed to the formation of a crystal–droplet (shell) interface. Although the assumption of a negligible change in the concentration of the solution phase is not strictly valid due to the finit system size, we confirme that the simplifie expression [Eq. (8)] yielded the values of ΔG_C^{max} that exhibits the same dependence on the size ratio σ_{AA}/σ_{BB} as those obtained from the original non-simplifie expression [Eq. (7)]. In Eq. (8), the activity of solute molecules $-\ln(1 - x_{Bs}) - \beta\phi_{Bs}^2$ and the interfacial tension γ_C are solvent-fraction-dependent. The Z_m term in the firs term represents the chemical potential difference during the solid–liquid transition of the pure solute and is expressed as a function of the degree of supercooling relative to the freezing point $T_m(n_L)$. The term of $-\ln(1 - x_{Bs}) - \beta\phi_{Bs}^2$ accounts for the reduction in this chemical potential difference caused by the incorporation of solvent molecules as an impurity into the liquid droplet. This phenomenon is referred to as freezing point depression in mixtures. As more solvent is incorporated into the droplet, the freezing point depression becomes more pronounced, increasing the crystallization barrier. In addition, as the solvent fraction of the droplet (shell) increases, the compositional difference between the shell and

the pure solute crystal core becomes larger. This enhances the dissimilarity between the two phases forming the crystal–droplet (shell) interface, resulting in a higher interfacial tension γ_C and further elevating the crystallization barrier. We conclude that an increase in the size ratio σ_{AA}/σ_{BB} results in a higher solvent fraction within the droplet, thereby leading to a more significan freezing point depression and an increase in crystal–droplet (shell) interfacial tension, both of which suppress crystallization.

D. Additive strategy for nucleation pathway control

As demonstrated by the results of this study and those in our previous study,[43] the system possesses a potential that exhibits a one-step pathway, when the degree of supercooling is sufficien to crystallize a pure solute liquid immediately. If the droplets formed from the solution closely resemble the pure solute, this potential is fully realized, resulting in a one-step pathway. However, if impurities are incorporated into the droplets, immediate crystallization is inhibited, and the system exhibits characteristics of a two-step pathway. This indicates that altering the composition of droplets and modifying their stability to crystallization offers a viable strategy to control the nucleation pathway. For example, introducing a third component into the droplets can shift the pathway from a one-step to a two-step process, as illustrated in Figs. 8(a) and 8(b).

We validated this strategy by conducting an additional series of simulations where additive LJ molecules C ($\varepsilon^*_{CC} = 0.67$, $\varepsilon^*_{AC} = 1.47$, $\varepsilon^*_{BC} = 0.067$, and $\sigma_{AA}/\sigma_{CC} = 1.15$) were introduced into each condition of parameter set 2. The additive molecule C was designed to be smaller than the solute molecules and have minimal interaction with the solvent, efficientl incorporating into the solute-rich droplets. ε^*_{CC} and ε^*_{AC} were tuned to prevent the phase separation of solute A and additive C within the droplet. Figures 3(a) and 3(b) show τ_C and n_L^{cryst} when 150 solvent molecules B were replaced with additive molecules C under each condition of parameter set 2. As expected, droplet crystallization was delayed under all conditions. For conditions with a larger σ_{AA}/σ_{BB}, the additive significantl suppressed crystallization and transformed the pathway from a one-step to a two-step process. For $\sigma_{AA}/\sigma_{BB} = 1.15$, crystallization was not observed within the 500 ns simulation time despite the crystal state being the most stable. This effect was attributed to the smaller solvent molecules for these conditions, which prevented the additive molecules from entering between solvent molecules, thereby facilitating their incorporation into solute-rich droplets. Similar scenarios, where third components (other than the monomer and solvent) induce two-step nucleation, are likely to occur in experimental systems because many particle synthesis processes involve supplying monomer molecules in combination with counterpart molecules that exhibit a high affinit for the monomer, such as in the form of salts or metal complexes. Although these counterpart molecules do not constitute the fina particle, their incorporation into intermediate structures can stabilize the intermediate structure and inhibit crystallization, thereby inducing the two-step pathway.

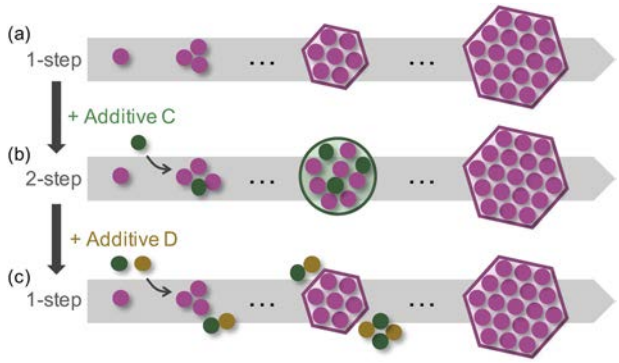

FIG. 8. Schematic of the strategy to control the nucleation pathway by introducing additive molecules.

This insight suggests the feasibility of a reverse approach. When a system exhibits a two-step pathway because of the inclusion of impurities in the intermediate structure, the removal of these impurities can aid in transitioning from a two-step pathway to a one-step pathway. This can be achieved, for example, by adding another additive molecule that interacts strongly with the impurity, as illustrated in Figs. 8(b) and 8(c). To validate this strategy, we performed a simulation in which we introduced another additive molecule D ($\varepsilon^*_{DD} = 1.34$, $\varepsilon^*_{AD} = 0.067$, $\varepsilon^*_{BD} = 1.34$, $\varepsilon^*_{CD} = 13.36$, and $\sigma_{AA}/\sigma_{DD} = 1$) to the system with $\sigma_{AA}/\sigma_{BB} = 1.10$, where the introduction of additive molecule C induced the two-step pathway. In contrast to additive molecule C, additive molecule D was designed to have minimal interaction with solute A and a considerably strong interaction with additive C. This design effectively inhibited the incorporation of additive C into solute-rich droplets. The star markers in Figs. 3(a) and 3(b) show τ_C and n_L^{cryst} when 300 solvent molecules B were replaced with 150 additive molecule C and 150 additive molecule D under the $\sigma_{AA}/\sigma_{BB} = 1.10$ condition of parameter set 2. The simulation result demonstrated that the introduction of additive D successfully restored the one-step pathway. This recovery was evident in the τ_C and n_L^{cryst} values, which returned to levels comparable with those observed prior to the introduction of additive C, i.e., the original parameter set 2 [Figs. 3(a) and 3(b)]. In fact, a similar strategy has been conducted in experimental systems. Green *et al.* reported that adding a primary amine during the synthesis of PbS nanoparticles using lead oleate and TMS-S [Bis(trimethylsilyl)sulfide alters the nucleation pathway from a stepwise process via intermediate clusters to a one-step process.[42] This pathway shift is attributed to the ability of primary amines to disrupt the interaction between metal ions and oleate ligands that stabilize the intermediate clusters. The additive effectively removes the ligands and presents the pure solute crystallization capability of solute monomers, thereby resulting in a one-step pathway. Thus, understanding the characteristics of intermediate structures and selecting suitable additives to modify their stability offers a versatile approach to control nucleation pathways.

The finding of this study are based on simulations of spherical molecules and, therefore, do not account for the effects of molecular orientation. However, the mechanisms of freezing point depression and interfacial tension increase caused by impurities apply universally, regardless of molecular shape, and are accordingly expected to manifest similarly even when the solute is anisotropic. In such cases, the presence of impurity molecules within the droplet may disrupt not only the positional arrangement but also the orientational order of solute molecules, potentially enhancing the suppression

of crystallization. Conversely, if an additive selectively promotes a particular molecular orientation, it would instead facilitate crystallization. Further investigation is needed to clarify the role of molecular orientation in these processes.

IV. CONCLUSION

We systematically investigated the effect of molecular size difference between the solute and solvent on crystallization from a droplet during a two-step nucleation process via LLPS using MD simulations of binary LJ systems. We explored crystallization behavior for two parameter sets, one with weaker solute–solute interactions and another with stronger interactions. We revealed that larger solute-to-solvent size ratios significantl delayed droplet crystallization in both cases. In the parameter set with strong solute–solute interactions, where crystallization typically occurs from smaller growing droplets, the droplet size at crystallization increased with an increase in the solute-to-solvent size ratio, resulting in a shift from a one-step-like nucleation pathway to a two-step-like pathway. The underlying mechanism is that the droplet composed of larger solute molecules incorporates more solvent molecules into the droplet, inhibiting crystallization.

We explained the change in droplet composition caused by the size ratio based on the change in the mixing free energy of the solute and solvent. When two molecules of different sizes are mixed, it is more thermodynamically favorable for a small amount of small molecules to mix into a larger quantity of larger molecules instead of the reverse. This is because the structure in which small molecules occupy gaps between large molecules enables the two types of molecules to mix without significantl disrupting the interactions between the large molecules. Consequently, this configu ration is advantageous both entropically and enthalpically. Larger solute molecules are more likely to form this type of structure, which leads to a higher solvent fraction in the droplet. Furthermore, we demonstrated that this increased solvent fraction correlates with a higher free energy barrier for droplet crystallization, as predicted by a thermodynamic model of the process. The model revealed that an increase in the molecular size ratio leads to a higher solvent composition in the droplet, which lowers the freezing point of droplet and raises the solid–liquid interfacial tension, ultimately delaying and suppressing crystallization.

Finally, we proposed a strategy to control the nucleation pathway using additives based on the above-mentioned findings We successfully incorporated these additives into the droplet and stabilized it to delay crystallization by introducing a small amount of additive molecules to the system that follows a one-step pathway, and we transformed the pathway into a two-step process. Conversely, it is possible to change the pathway to a one-step pathway by adding molecules that strongly interact with molecules stabilizing the intermediate state. We believe that selecting appropriate additives to modify the stability of intermediates is a promising strategy to control nucleation pathways in various systems, and this study provides fundamental guidelines for implementing such an approach.

ACKNOWLEDGMENTS

This work was partially supported by the JSPS Grant-in-Aid for Scientifi Research (B) (Grant No. 20H02504), Grant-in-Aid for JSPS Fellows (Grant No. 21J23476), and Information Center of Particle Technology, Japan.

AUTHOR DECLARATIONS

Conflict of Interest

The authors have no conflict to disclose.

Author Contributions

Y.I. and S.W. designed the study and prepared the manuscript. Y.I. conducted the simulations and analyses. S.W. and S.H. provided instructions as supervisors.

Yuya Iida: Conceptualization (equal); Investigation (lead); Writing – original draft (lead). **Shotaro Hiraide**: Supervision (equal). **Satoshi Watanabe**: Conceptualization (equal); Supervision (lead); Writing – review & editing (lead).

DATA AVAILABILITY

The data that support the finding of this study are available from the corresponding author upon reasonable request.

APPENDIX: DETAILS ON INDUCTION TIME AND FREE ENERGY CHANGE

1. Calculation of induction time and its average

The induction time and its average value were calculated as reported in our previous study.[43,44] We define the induction time of liquid-droplet formation t_L as the time until $n_L(t) \geq 30$ and $n_{L,\,\min} > 0.6 n_L(t)$ were satisfied where $n_{L,\,\min}$ represents the minimum value of n_L among all n_L after time t. We define the induction time of crystallization t_C as the time until $n_C \geq 30$ and $n_{C,\,\min} > 0.6 n_C(t)$ were satisfie after the liquid-droplet formation $(t = t_L)$, where $n_{C,\,\min}$ represents the minimum value of n_C among all n_C after time t.

Then, we calculated the average induction time of crystallization τ_C of N_{run} (=20 or more) runs based on the survival probability of the crystal-free state, which is define as

$$P(t) = \frac{N_{cfree}(t)}{N_{run}}, \tag{A1}$$

where $N_{cfree}(t)$ represents the number of runs that have not formed a crystal at time t. By assuming that stochastic crystal nucleation within a droplet follows a Poisson process, $P(t)$ can be expressed as

$$P(t) = \exp\left(-\frac{t}{\tau_C}\right). \tag{A2}$$

The average induction time of crystallization τ_C of N_{run} runs can be calculated by fittin $P(t)$ using Eqs. (A1) and (A2). However, it is not always feasible to obtain the simulated values of $P(t)$ because some simulation runs do not form a crystal within a maximum simulation time of 500 ns. We accordingly calculate τ_C in the following three cases, depending on the number of runs, $n_{nuc}(\leq N_{run})$, in which a crystal formation is observed.

Case 1: $2 \le n_{nuc} \le N_{run}$

In this case, we obtain n_{nuc} data points for $P(t)$ using Eq. (A1) and then calculate τ_{L} by fittin the n_{nuc} data points using Eq. (A2).

Case 2: $n_{\mathrm{nuc}} = 1$

In this case, we obtain only one data point for $P(t) = 1$ at $t = t_{\mathrm{C}}$ using Eq. (A1). This data point for $P(t_{\mathrm{C}}) = 1$ is not suitable for fittin because Eq. (A2) provides $P(t_{\mathrm{L}}) = 1$ only in the case of $\tau_{\mathrm{C}} \to \infty$. Instead of fittin using Eq. (A2), we compute the simulated $P(t_{\mathrm{L}})$ as

$$P(t_{\mathrm{C}}) = 1 - \frac{1}{N_{\mathrm{run}}}, \tag{A3}$$

which implies that we interpreted the simulation results as a crystal generated within time t_{C} with a probability of $1/N_{\mathrm{run}}$. We calculate τ_{C} as a value such that Eq. (A2) satisfie Eq. (A3).

Case 3: $n_{\mathrm{nuc}} = 0$.

In this case, no data points are obtained for $P(t)$. The only known observation is that no crystals are produced within the maximum simulation time of 500 ns. We estimate a lower limit of τ_{C} using the same procedure as Case 2 by assuming that a crystal forms at $t = 500$ ns in one of the simulation runs.

2. Detailed expression of $\Delta G(n_{\mathrm{L}}, n_{\mathrm{C}})$

The free energy change due to the formation of a core–shell nucleus $\Delta G(n_{\mathrm{L}}, n_{\mathrm{C}})$ with an n_{C}-sized core and an $(n_{\mathrm{L}} - n_{\mathrm{C}})$-sized shell from the initial solution phase was calculated using a model we developed in our previous study[43] as follows:

$$\Delta G(n_{\mathrm{L}}, n_{\mathrm{C}}) = \Delta G_{\mathrm{V}} + \Delta G_{\mathrm{S}}, \tag{A4}$$

where ΔG_{V} represents a volume term, which is the stabilization term owing to the formation of a new stable phase, and ΔG_{S} represents an interface term, the energy penalty term because of interface formation. Considering the composition change in the solution phase during the nucleation, the volume term ΔG_{V} is expressed as

$$\begin{aligned}\Delta G_{\mathrm{V}} = {} & n_{\mathrm{C}} k_{\mathrm{B}} T\left[-Z_{\mathrm{m}}\varepsilon^{*}_{\mathrm{AA}}\left(\frac{T_{\mathrm{m}} - T}{T_{\mathrm{m}}}\right) - \ln x_{\mathrm{Aa}} - \beta{\phi_{\mathrm{Ba}}}^{2}\right] \\ & + (n_{\mathrm{L}} - n_{\mathrm{C}}) k_{\mathrm{B}} T\left[\frac{\sum x_{is}\,\ln\left(x_{is}/x_{ia}\right)}{x_{\mathrm{As}}} - \beta\frac{\left(\phi_{\mathrm{As}} - \phi_{\mathrm{Aa}}\right)^{2}}{\phi_{\mathrm{As}}}\right] \\ & + N_{\mathrm{A}} k_{\mathrm{B}} T\left[\frac{\sum x_{i0}\,\ln\left(x_{ia}/x_{i0}\right)}{x_{\mathrm{A0}}} + \beta\frac{\left(\phi_{\mathrm{Aa}} - \phi_{\mathrm{A0}}\right)^{2}}{\phi_{\mathrm{A0}}}\right], \end{aligned} \tag{A5}$$

$$\text{with} \quad \phi_{\mathrm{A}} = \frac{x_{\mathrm{A}}}{x_{\mathrm{A}} + r x_{\mathrm{B}}}, \quad \phi_{\mathrm{B}} = \frac{r x_{\mathrm{B}}}{x_{\mathrm{A}} + r x_{\mathrm{B}}},$$

where Z_{m} represents the fusion enthalpy of the LJ molecules scaled by ε; x_{i0} and ϕ_{i0} $(i = \mathrm{A}, \mathrm{B})$ represent mole and volume fractions of solute in the initial solution phase, respectively; x_{ia} and ϕ_{ia} $(i = \mathrm{A}, \mathrm{B})$ represent mole and volume fractions of solute in the solution phase after the nucleation, respectively; N_{A} represents the number of solute molecules in the system; and T_{m} represents the freezing point of the droplet, which is expressed as a function of the droplet size n_{L} considering the Gibbs–Thomson effect as

$$T_{\mathrm{m}} = T_{\mathrm{mb}}\left(1 - \frac{2\gamma_{\mathrm{C}} a_{\mathrm{C}}^{2/3}}{3k_{\mathrm{B}} T Z_{\mathrm{m}} \varepsilon^{*}_{\mathrm{AA}} n_{\mathrm{L}}^{1/3}}\right), \tag{A6}$$

where T_{mb} represents the freezing point of the bulk crystal of solute, $a_{\mathrm{C}} = 6\sqrt{\pi} v_{\mathrm{C}}$, v_{C} represents the occupied volume per solute molecule in a crystal, and γ_{C} represents the crystal–shell interfacial tension.

The interface term ΔG_{S} is expressed as

$$\begin{aligned}\Delta G_{\mathrm{V}} = {} & \gamma_{\mathrm{L}} a_{\mathrm{L}}^{2/3}\left\{(n_{\mathrm{L}} - n_{\mathrm{C}})\left(1 + \frac{r x_{\mathrm{Bs}}}{x_{\mathrm{As}}}\right) + n_{\mathrm{C}}\frac{v_{\mathrm{C}}}{v_{\mathrm{L}}}\right\}^{2/3} \\ & + \gamma_{\mathrm{C}} a_{\mathrm{C}}^{2/3} n_{\mathrm{C}}^{2/3}, \end{aligned} \tag{A7}$$

where γ_{L} represents the solution–droplet (shell) interfacial tension, $a_{\mathrm{L}} = 6\sqrt{\pi} v_{\mathrm{L}}$, and v_{L} represents the occupied volume per solute molecule in a liquid phase.

REFERENCES

[1] T. Ishida, T. Murayama, A. Taketoshi, and M. Haruta, "Importance of size and contact structure of gold nanoparticles for the genesis of unique catalytic processes," Chem. Rev. **120**, 464–525 (2020).

[2] C. Xie, Z. Niu, D. Kim, M. Li, and P. Yang, "Surface and interface control in nanoparticle catalysis," Chem. Rev. **120**, 1184–1249 (2020).

[3] P. Khadka, J. Ro, H. Kim, I. Kim, J. T. Kim, H. Kim, J. M. Cho, G. Yun, and J. Lee, "Pharmaceutical particle technologies: An approach to improve drug solubility, dissolution and bioavailability," Asian J. Pharm. Sci. **9**, 304–316 (2014).

[4] S. I. Hamdallah, R. Zoqlam, P. Erfle M. Blyth, A. M. Alkilany, A. Dietzel, and S. Qi, "Microfluidic for pharmaceutical nanoparticle fabrication: The truth and the myth," Int. J. Pharm. **584**, 119408 (2020).

[5] M. Liu, N. Yazdani, M. Yarema, M. Jansen, V. Wood, and E. H. Sargent, "Colloidal quantum dot electronics," Nat. Electron. **4**, 548–558 (2021).

[6] C. R. Kagan, L. C. Bassett, C. B. Murray, and S. M. Thompson, "Colloidal quantum dots as platforms for quantum information science," Chem. Rev. **121**, 3186–3233 (2021).

[7] D. Kashchiev, *Nucleation Basic Theory with Applications* (Butterworth–Heinemann, 2000).

[8] P. R. t. Wolde and D. Frenkel, "Enhancement of protein crystal nucleation by critical density fluctuations, Science **277**, 1975–1978 (1997).

[9] J. F. Lutsko and G. Nicolis, "Theoretical evidence for a dense flui precursor to crystallization," Phys. Rev. Lett. **96**, 046102 (2006).

[10] J. R. Savage and A. D. Dinsmore, "Experimental evidence for two-step nucleation in colloidal crystallization," Phys. Rev. Lett. **102**, 198302 (2009).

[11] P. G. Vekilov, "The two-step mechanism of nucleation of crystals in solution," Nanoscale **2**, 2346–2357 (2010).

[12] E. Wiedenbeck, M. Kovermann, D. Gebauer, and H. Cölfen, "Liquid metastable precursors of ibuprofen as aqueous nucleation intermediates," Angew. Chem., Int. Ed. **58**, 19103–19109 (2019).

[13] D. Gebauer, A. Völkel, and H. Cölfen, "Stable prenucleation calcium carbonate clusters," Science **322**, 1819–1822 (2008).

[14] E. M. Pouget, P. H. H. Bomans, J. A. C. M. Goos, P. M. Frederik, G. de With, and N. A. J. M. Sommerdijk, "The initial stages of template-controlled $CaCO_3$ formation revealed by cryo-TEM," Science **323**, 1455–1458 (2009).

[15] R. Demichelis, P. Raiteri, J. D. Gale, D. Quigley, and D. Gebauer, "Stable prenucleation mineral clusters are liquid-like ionic polymers," Nat. Commun. **2**, 590 (2011).

[16] J. Scheck, B. Wu, M. Drechsler, R. Rosenberg, A. E. S. Van Driessche, T. M. Stawski, and D. Gebauer, "The molecular mechanism of iron(III) oxide nucleation," J. Phys. Chem. Lett. **7**, 3123–3130 (2016).

[17] E. Ruiz-Agudo, A. Burgos-Cara, C. Ruiz-Agudo, A. Ibañez-Velasco, H. Cölfen, and C. Rodriguez-Navarro, "A non-classical view on calcium oxalate precipitation and the role of citrate," Nat. Commun. **8**, 768 (2017).

[18]J. T. Avaro, S. L. P. Wolf, K. Hauser, and D. Gebauer, "Stable prenucleation calcium carbonate clusters defin liquid–liquid phase separation," Angew. Chem., Int. Ed. **59**, 6155–6159 (2020).
[19]R. L. Penn and J. F. Banfield "Imperfect oriented attachment: Dislocation generation in defect-free nanocrystals," Science **281**, 969–971 (1998).
[20]M. Niederberger and H. Cölfen, "Oriented attachment and mesocrystals: Non-classical crystallization mechanisms based on nanoparticle assembly," Phys. Chem. Chem. Phys. **8**, 3271–3287 (2006).
[21]F. Wang, V. N. Richards, S. P. Shields, and W. E. Buhro, "Kinetics and mechanisms of aggregative nanocrystal growth," Chem. Mater. **26**, 5–21 (2014).
[22]J. J. De Yoreo, P. U. P. A. Gilbert, N. A. J. M. Sommerdijk, R. L. Penn, S. Whitelam, D. Joester, H. Zhang, J. D. Rimer, A. Navrotsky, J. F. Banfield A. F. Wallace, F. M. Michel, F. C. Meldrum, H. Cölfen, and P. M. Dove, "Crystallization by particle attachment in synthetic, biogenic, and geologic environments," Science **349**, aaa6760 (2015).
[23]M. Takasuga and H. Ooshima, "Control of crystal size during oiling out crystallization of an API," Cryst. Growth Des. **14**, 6006–6011 (2014).
[24]M. Takasuga and H. Ooshima, "Control of crystal aspect ratio and size by changing solvent composition in oiling out crystallization of an active pharmaceutical ingredient," Cryst. Growth Des. **15**, 5834–5838 (2015).
[25]M. Sun, S. Du, M. Chen, S. Rohani, H. Zhang, Y. Liu, P. Sun, Y. Wang, P. Shi, S. Xu, and J. Gong, "Oiling-out investigation and morphology control of β-alanine based on ternary phase diagrams," Cryst. Growth Des. **18**, 818–826 (2018).
[26]M. Sun, W. Tang, S. Du, Y. Zhang, X. Fu, and J. Gong, "Understanding the roles of oiling-out on crystallization of β-alanine: Unusual behavior in metastable zone width and surface nucleation during growth stage," Cryst. Growth Des. **18**, 6885–6890 (2018).
[27]S. Wang, Y. Liu, S. Guo, H. Yan, K. Li, L. Tong, T. Li, M. Chen, Z. Gao, and J. Gong, "Design of single and multicomponent drug spherical particles with improved powder properties in water instead of organic solvents: A case study of gemfibrozil, ACS Sustainable Chem. Eng. **10**, 12411–12422 (2022).
[28]Y. Liu, Y. Ma, C. Yu, Y. Gao, K. Li, L. Tong, M. Chen, and J. Gong, "Spherical agglomeration of high melting point drugs in water at low temperature by developing a two-step oiling-out mechanism and the design strategy," Green Chem. **24**, 5779–5791 (2022).
[29]F. C. N. Firth, M. W. Gaultois, Y. Wu, J. M. Stratford, D. S. Keeble, C. P. Grey, and M. J. Cliffe, "Exploring the role of cluster formation in UiO family Hf metal–organic frameworks with *in situ* X-ray pair distribution function analysis," J. Am. Chem. Soc. **143**, 19668–19683 (2021).
[30]J. Xing, L. Schweighauser, S. Okada, K. Harano, and E. Nakamura, "Atomistic structures and dynamics of prenucleation clusters in MOF-2 and MOF-5 syntheses," Nat. Commun. **10**, 3608 (2019).
[31]N. Duff and B. Peters, "Nucleation in a Potts lattice gas model of crystallization from solution," J. Chem. Phys. **131**, 184101 (2009).
[32]C. Guo, J. Wang, J. Li, Z. Wang, and S. Tang, "Kinetic pathways and mechanisms of two-step nucleation in crystallization," J. Phys. Chem. Lett. **7**, 5008–5014 (2016).
[33]Arjun, T. A. Berendsen, and P. G. Bolhuis, "Unbiased atomistic insight in the competing nucleation mechanisms of methane hydrates," Proc. Natl. Acad. Sci. U. S. A. **116**, 19305–19310 (2019).
[34]A. Kumar and V. Molinero, "Two-step to one-step nucleation of a zeolite through a metastable gyroid mesophase," J. Phys. Chem. Lett. **9**, 5692–5697 (2018).
[35]J. Li, Y. Li, Q. Li, Z. Wang, and F. Leonard Deepak, "Atomic-scale dynamic observation reveals temperature-dependent multistep nucleation pathways in crystallization," Nanoscale Horiz. **4**, 1302–1309 (2019).
[36]C. Li, Z. Liu, E. C. Goonetilleke, and X. Huang, "Temperature-dependent kinetic pathways of heterogeneous ice nucleation competing between classical and non-classical nucleation," Nat. Commun. **12**, 4954 (2021).
[37]M. Salvalaglio, C. Perego, F. Giberti, M. Mazzotti, and M. Parrinello, "Molecular-dynamics simulations of urea nucleation from aqueous solution," Proc. Natl. Acad. Sci. U. S. A. **112**, E6–E14 (2015).
[38]M. Salvalaglio, M. Mazzotti, and M. Parrinello, "Urea homogeneous nucleation mechanism is solvent dependent," Faraday Discuss. **179**, 291–307 (2015).
[39]Q. Hu, M. H. Nielsen, C. L. Freeman, L. M. Hamm, J. Tao, J. R. I. Lee, T. Y. J. Han, U. Becker, J. H. Harding, P. M. Dove, and J. J. De Yoreo, "The thermodynamics of calcite nucleation at organic interfaces: Classical vs. non-classical pathways," Faraday Discuss. **159**, 509–523 (2012).
[40]A. R. Lauer, M. A. Durán-Olivencia, A. Fernandez-Martinez, and A. E. S. Van Driessche, "Multistep nucleation compatible with a single energy barrier: Catching the non-classical culprit," Faraday Discuss. **235**, 95–108 (2022).
[41]A. Dreyer, K. Eckstädt, T. Koop, P. Jutzi, and A. Hütten, "Surface stabilization determines a classical versus non-classical nucleation pathway during particle formation," RSC Adv. **6**, 74061–74066 (2016).
[42]P. B. Green, P. Narayanan, Z. Li, P. Sohn, C. J. Imperiale, and M. W. B. Wilson, "Controlling cluster intermediates enables the synthesis of small PbS nanocrystals with narrow ensemble line widths," Chem. Mater. **32**, 4083–4094 (2020).
[43]Y. Iida, T. Hiratsuka, M. T. Miyahara, and S. Watanabe, "Mechanism of nucleation pathway selection in binary Lennard-Jones solution: A combined study of molecular dynamics simulation and free energy analysis," J. Phys. Chem. B **127**, 3524–3533 (2023).
[44]Y. Iida, S. Hiraide, M. T. Miyahara, and S. Watanabe, "Solute interaction-driven and solvent interaction-driven liquid–liquid phase separation induced by molecular size difference," J. Chem. Phys. **160**, 044504 (2024).
[45]S. Boothroyd, A. Kerridge, A. Broo, D. Buttar, and J. Anwar, "Why do some molecules form hydrates or solvates?," Cryst. Growth Des. **18**, 1903–1908 (2018).
[46]J. Anwar, S. Khan, and L. Lindfors, "Secondary crystal nucleation: Nuclei breeding factory uncovered," Angew. Chem., Int. Ed. **54**, 14681–14684 (2015).
[47]J. Anwar, P. K. Boateng, R. Tamaki, and S. Odedra, "Mode of action and design rules for additives that modulate crystal nucleation," Angew. Chem., Int. Ed. **48**, 1596–1600 (2009).
[48]K. Maeda, T. Miki, K. Itoh, K. Arafune, T. Yamamoto, and K. Fukui, "Anti-solvent crystallization of a ternary Lennard–Jones mixture performed by molecular dynamics," J. Mol. Liq. **209**, 1–5 (2015).
[49]G. A. Tribello, F. Giberti, G. C. Sosso, M. Salvalaglio, and M. Parrinello, "Analyzing and driving cluster formation in atomistic simulations," J. Chem. Theory Comput. **13**, 1317–1327 (2017).
[50]G. Bussi, D. Donadio, and M. Parrinello, "Canonical sampling through velocity rescaling," J. Chem. Phys. **126**, 014101 (2007).
[51]M. Parrinello and A. Rahman, "Polymorphic transitions in single crystals: A new molecular dynamics method," J. Appl. Phys. **52**, 7182 (1981).
[52]H. J. C. Berendsen, D. van der Spoel, and R. van Drunen, "GROMACS: A message-passing parallel molecular dynamics implementation," Comput. Phys. Commun. **91**, 43–56 (1995).
[53]G. A. Tribello, M. Bonomi, D. Branduardi, C. Camilloni, and G. Bussi, "PLUMED 2: New feathers for an old bird," Comput. Phys. Commun. **185**, 604–613 (2014).
[54]A. Stukowski, "Visualization and analysis of atomistic simulation data with OVITO–The open visualization tool," Modell. Simul. Mater. Sci. Eng. **18**, 015012 (2010).
[55]J. H. Hildebrand and R. L. Scott, *Regular Solutions* (Prentice-Hall, Englewood Cliffs, NJ, 1962).
[56]C. L. Jackson and G. B. McKenna, "The melting behavior of organic materials confine in porous solids," J. Chem. Phys. **93**, 9002 (1990).